Inorganic Chemistry

Article

pubs.acs.org/IC

$(Ni,Mg)_3Si_2O_5(OH)_4$ Solid-Solution Nanotubes Supported by Sub-0.06 wt % Palladium as a Robust High-Efficiency Catalyst for Suzuki–Miyaura Cross-Coupling Reactions

Wancheng Zhu, Yan Yang, Shi Hu, Guolei Xiang, Biao Xu, Jing Zhuang, and Xun Wang*

Department of Chemistry, Tsinghua University, Beijing, 100084, People's Republic of China

Supporting Information

ABSTRACT: $(Ni_{1-x}Mg_x)_3Si_2O_5(OH)_4$ solid-solution nanotubes (NTs) with tunable compositions were hydrothermally synthesized by altering the molar ratio of Mg^{2+} to Ni^{2+}. The as-synthesized NTs were loaded with sub-0.06 wt % palladium (Pd; ~0.045 wt %) for Suzuki–Miyaura (SM) coupling reactions between iodobenzene or 4-iodotoluene and phenylboronic acid. The $(Ni,Mg)_3Si_2O_5(OH)_4$ (Mg^{2+}:Ni^{2+} = 1.0:1.0) NTs supported by 0.045 wt % Pd promoted the iodobenzene-participated coupling reaction with a high yield of >99%, an excellent recycling catalytic performance during 10 cycles of catalysis with yields of ~99%, and also an extremely low Pd releasing level of ~0.02 ppm. High-activity Pd and PdO clusters, multitudes of dislocations, and defects and terraces contained within the NTs should contribute to the $(Ni,Mg)_3Si_2O_5(OH)_4$ (Mg^{2+}:Ni^{2+} = 1.0:1.0) NTs supported by 0.045 wt % Pd as a robust, reusable, and high-efficiency catalyst for SM coupling reactions with an extremely low Pd releasing level. The present hydrothermally stable $(Ni,Mg)_3Si_2O_5(OH)_4$ (Mg^{2+}:Ni^{2+} = 1.0:1.0) solid-solution silicate NTs provided an ideal alternative tubular-structured support for noble- or transition-metal catalysts with low Pd loading, good recycling, and extremely low ppb levels of Pd release, which could also be extended to some other SM coupling reactions.

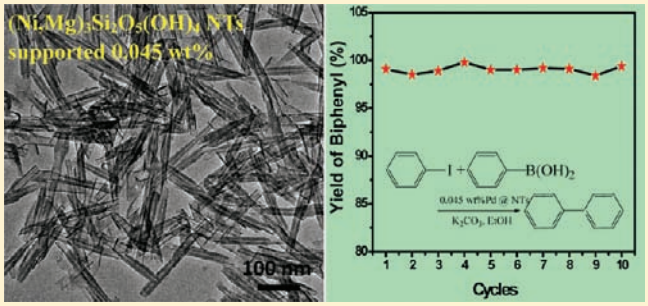

INTRODUCTION

In the past few decades, palladium (Pd)-catalyzed carbon–carbon (C–C) coupling reactions including Heck,[1−3] Negishi,[4,5] Sonogashira,[6,7] etc., have been paid worldwide attention and employed versatilely for the distinguished cornerstone position within modern organic synthesis. Among the various C–C couplings, Suzuki–Miyaura (SM) couplings have attracted particular concerns, have been considered as one of the most efficient synthetic routes to biaryl compounds, and have thus been extensively employed in academic laboratories as well as pharmaceutical and fine-chemical industries.[8−11] Compared with other C–C bond construction reactions, the mainstay and popularity of SM couplings was based on several unique advantages,[12,13] such as the required relatively mild reaction conditions, commercial availability of the starting diverse boronic acids, tolerance of a variety of functional groups as starting partners, ease of handling/removal of boron-bearing byproducts, and in some cases environmental benign character for accessibility in aqueous media.[10,14]

Homogeneous Pd-catalyzed C–C coupling reactions have been extensively studied for their excellent activity and selectivity, which, however, suffers from a number of drawbacks, especially in the removal and reuse of the catalyst. This leads to the unavoidable loss of expensive metal and ligands and also resultant product contamination, which has emerged as an acute issue for large-scale synthesis, especially in the pharmaceutical industry.[10] To cope with these burning issues, heterogeneous Pd catalysis has been a promising option,[8,10] and recyclable/reusable Pd catalysts have emerged as an alternative competitive solution.[15] For heterogeneous Pd catalysis, Pd is generally immobilized on a solid support, and the particle size, surface area, pore structure, and acid–base properties of the support usually have an impact on the activity of the catalytic system.[8] Up to now, great efforts have been made to develop new catalyst carriers and high-activity Pd species for the referred SM reactions. For example, activated carbon (charcoal),[16] zeolites, molecular sieves, metal oxides (silica, alumina, MgO, ZnO, etc.), layered clays,[17] alkaline-earth carbonates ($CaCO_3$, $BaCO_3$, $SrCO_3$, etc.), and organic polymers,[18] etc., have been found as effective Pd supports. In many cases, however, the hydrothermal stability of the support, e.g., mesoporous silica with amorphous walls, still remained a great challenge. The amorphous walls of the support could easily be destroyed by the base used for the reaction, resulting in a collapse of the mesoporous structure. In addition, a 5 wt % or even higher Pd loading is generally used for most of the Pd catalysts.[8] Pd on charcoal (Pd/C) is by far the most often used heterogeneous Pd catalyst for coupling reactions, and the commercially available Pd/C catalysts contain a Pd content of 1–20%. Nonetheless, the Pd/C catalyst suffers from relatively

Received: November 13, 2011
Published: May 14, 2012

   dx.doi.org/10.1021/ic2024378 | Inorg. Chem. 2012, 51, 6020–6031

severe Pd leaching; e.g., leaching up to 14% Pd was observed in Heck reactions.[8] Recently, novel Pd species have also been reported, such as Pd nanoparticles (NPs),[9,19] colloidal Pd,[20,21] and Pd clusters.[22,23] Reducing the Pd employed by minimizing Pd leaching and residual species within the product is of great significance especially for pharmaceutical and fine-chemical synthesis. To date, it is still a challenge to develop novel support for Pd as a high-efficiency catalyst for heterogeneous C−C cross-coupling reactions with low loading, high activity, and low leaching.

In this work, $(Ni_{1-x},Mg_x)_3Si_2O_5(OH)_4$ solid-solution nanotubes (NTs) with tunable compositions were hydrothermally synthesized, among which the $(Ni,Mg)_3Si_2O_5(OH)_4$ (Mg^{2+}:Ni^{2+} = 1.0:1.0) NTs were loaded with sub-0.06 wt % Pd (~0.045 wt %) for the SM coupling reactions between iodobenzene or 4-iodotoluene and phenylboronic acid. The low level of Pd loading, the low ppb level of Pd release, and the excellent hydrothermal stability of the nanotubular support without destruction after 10 cycles of high-efficiency catalysis definitely indicated that, the as-synthesized solid-solution NTs supported by 0.045 wt % Pd were an ideal robust catalyst for the selected SM coupling reactions, which could also be extended as a competitive reusable high-efficiency catalyst for some other SM coupling reactions.

EXPERIMENTAL SECTION

1. Synthesis of $(Ni_{1-x},Mg_x)_3Si_2O_5(OH)_4$ NTs. All reagents were of analytical grade and were used directly without further purification. $(Ni,Mg)_3Si_2O_5(OH)_4$ NTs (Mg^{2+}:Ni^{2+} = 1.0:1.0) were synthesized by a facile hydrothermal route. In a typical procedure, 1.0 mmol of $Mg(NO_3)_2{\cdot}6H_2O$ and 1.0 mmol of $NiCl_2{\cdot}6H_2O$ were dissolved into 30 mL of deionized (DI) water under constant magnetic stirring at room temperature. A total of 15.39 mL of liquid $Na_2O{\cdot}nSiO_3$ (n = 3.1−3.4) was dissolved and adjusted to 100 mL of mixed solution. Then 4.0 mL of the previous solution was added to the preprepared magnetically stirred system, resulting in a gray-green slurry. After ca. 10 min of stirring, 5.8 g of NaOH was poured into the resultant slurry, with the color changing to a grayer green. Stirred for another 10 min, the as-obtained slurry was transferred to a Teflon-lined stainless steel autoclave with a capacity of 45.0 mL. The autoclave was sealed, heated to 210 °C (heating rate: 5 °C min^{-1}), and kept in an isothermal state for 24.0 h. After hydrothermal synthesis, the autoclave was cooled to room temperature naturally, and the as-synthesized precipitate was washed with DI water and separated by centrifugation (10000 rpm, 20.0 min) three times and then dried at 80 °C for 24.0 h for further characterization and evaluation. To evaluate the effect of the relative amount of Mg^{2+} and Ni^{2+} on the composition and morphology of the hydrothermal product, the molar ratios of Mg^{2+} and Ni^{2+} were altered within the range of 0:2.0 to 2.0:0, keeping the whole amount of Mg^{2+} and Ni^{2+} as 2.0 moles and other conditions unchanged.

2. Loading of sub-0.06 wt % Pd. Typically, 0.2 g of the as-synthesized NTs was added into the solution containing 20.0 mL of ethanol and 30.0 mL of DI water within a three-neck flask equipped with a condenser under constant magnetic stirring. The flask was heated within a preheated oil bath to the boiling state (ca. 110 °C), followed by a rapid injection of 22.54 μL of a $PdCl_2$ solution (0.05 mol L^{-1}), and refluxed for 0.5 h in the absence of protection of inert gas, with a theoretical 0.06 wt % Pd versus the NTs to be loaded. Then the system was stopped and separated by centrifugation (10000 rpm, 20.0 min), to the liquid phase was added ca. 0.4 g of $NaBH_4$ to monitor whether all of the Pd^{2+} ions have been reduced, and the solid phase (i.e., NTs supported by the sub-0.06 wt % Pd catalyst used hereafter) was washed with ethanol for a second time and finally collected for catalytic evaluation.

3. Catalytic Performance of the $(Ni_{1-x},Mg_x)_3Si_2O_5(OH)_4$ NTs Supported by Sub-0.06 wt % Pd. In a first typical SM coupling reaction, 1.5 mmol of phenylboronic acid, 2.0 mmol of K_2CO_3, previously collected NTs supported by sub-0.06 wt % Pd, 15.0 mL of ethanol, and 1.0 mmol of iodobenzene were mixed within a three-neck flask, then heated to 70 °C, and kept in an isothermal state for 3.0 h, within a preheated oil bath. After the reaction, the liquid product phase was separated from the solid phase by centrifugation (10000 rpm, 20.0 min) and set aside for further characterization. For the specific $(Ni,Mg)_3Si_2O_5(OH)_4$ (molar ratio of Mg^{2+}:Ni^{2+} = 1.0:1.0) NTs, to evaluate the recycling catalytic performance, the solid catalyst phase after the previous centrifugation was washed with 40.0 mL of DI water to eliminate K_2CO_3, separated by centrifugation, then washed with 20.0 mL of ethanol to substitute remanent DI water, separated by centrifugation, and finally transferred to the next loop of catalysis by adding 15.0 mL of ethanol, followed by introduction of the same amount of fresh phenylboronic acid, iodobenzene, and K_2CO_3, under the same reactant conditions. In addition, for the NTs with a molar ratio of Mg^{2+}:Ni^{2+} = 1.0:1.0, a second SM coupling reaction between 4-iodotoluene (1.0 mmol) and phenylboronic acid (1.5 mmol) was also carried out under the same conditions as those described previously, using the NTs supported by sub-0.06 wt % Pd as the catalyst. For comparison, a blank test corresponding to the first SM coupling reaction was performed using the same amount of bare $(Ni,Mg)_3Si_2O_5(OH)_4$ (molar ratio of Mg^{2+}:Ni^{2+} = 1.0:1.0) NTs without Pd loading as the catalyst, with other conditions unchanged. To investigate the possible migration and mechanism of the trace Pd during the SM coupling reaction, the reaction system was interrupted when proceeded at 70 °C for ca. 0.5 h and then quenched by room temperature water or cooled naturally to room temperature by raising the flask out of the oil bath in due course, followed by centrifugation as previously.

4. Mercury Poisoning Experiment. The mercury poisoning test was carried out in the process of catalysis, with $(Ni,Mg)_3Si_2O_5(OH)_4$ (molar ratio of Mg^{2+}:Ni^{2+} = 1.0:1.0) NTs supported by sub-0.06 wt % Pd as the catalyst. All reactants, base, solvent, and NTs supported by a catalyst were reduced by half of those employed in the precedent typical SM coupling reaction. When the catalysis proceeded at 70 °C for 15.0 min with an approximate conversion of ca. 15−50%, the flask was raised out of the oil bath and quenched by room temperature water (~22 °C) rapidly. After centrifugation, the supernatant was sampled ~500 μL for gas chromatography (GC)-mass spectrometry (MS), then the residual catalytic system was shaked up and thoroughly transferred to the flask and added by a mercury bead with a diameter of ~2.6 mm. The flask was sealed and vigorously stirred magnetically within a working fume hood for 12.0 h, to ensure excellent mixing. Then the flask was recovered to 70 °C for another 2.0 h and 45.0 min. Finally, the flask was cooled naturally to room temperature, and the liquid product phase was collected after centrifugation, with the remanent solid phase including mercury beads deposited on the bottom of the flask post-treated with sulfur for security.

5. Characterization. The structure of the sample was identified by a powder X-ray diffractometer (D8-Advance, Bruker, Germany) using Cu Kα radiation (λ = 1.54178 Å) and a fixed power source (40.0 kV; 40.0 mA). The morphology and microstructure of the samples were examined by a high-resolution transmission electron microscope (JEM-2010, JEOL, Japan, at 120.0 kV). High-angle annular dark-field (HAADF) scanning transmission electron microscopy (STEM) and elemental mapping were determined by a high-resolution transmission electron microscope (Tecnai G2 F20 S-Twin, FEI, USA, at 200.0 kV) equipped with a Fischione accessory. Optical properties were examined by a UV−vis spectrophotometer (UV-3600 230VCE, Shimadzu, Japan) with an integrating sphere accessory. The actual amount of Pd loaded on the NTs and also that of the liquid product phase derived from the first SM coupling reaction were determined by inductively coupled plasma mass spectrometry (ICP-MS) analysis (XSeries 2, Thermo Fisher, USA). N_2 adsorption−desorption isotherms were measured using a chemisorption−physisorption analyzer (Autosorb-1, Quantachrome, USA) at 77 K after the samples had been outgassed at 200 °C for 120 min. The specific surface area was calculated from the adsorption branches in the relative pressure range of 0.10−0.31 using the multipoint Brunauer−Emmett−Teller (BET) method, and the pore-size distribution was evaluated from the

dx.doi.org/10.1021/ic2024378 | Inorg. Chem. 2012, 51, 6020−6031

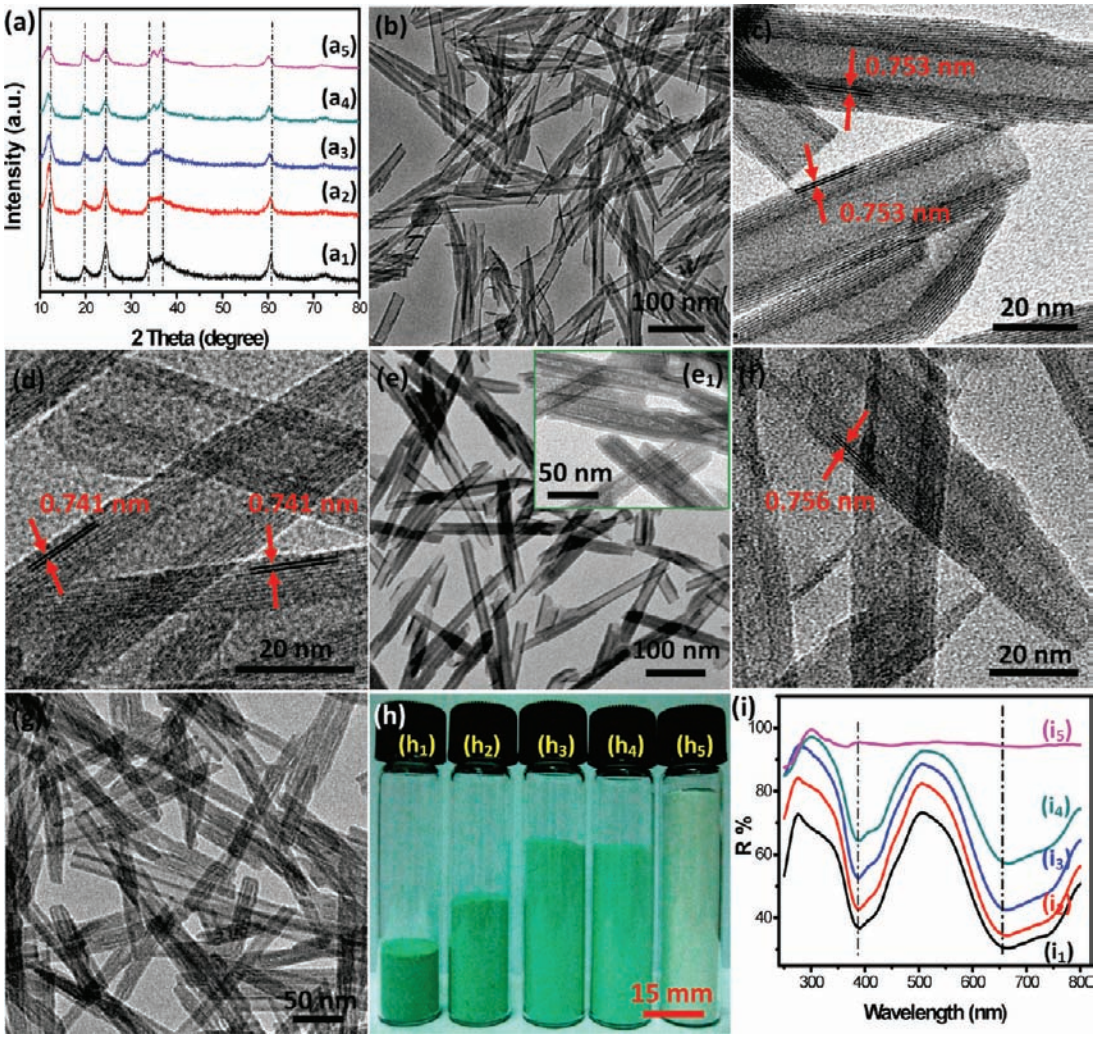

Figure 1. XRD patterns (a), TEM images (b–g), digital pictures (h), and UV–vis diffuse-reflectance spectra (i) of the hydrothermally synthesized $(Ni_{1-x},Mg_x)_3Si_2O_5(OH)_4$ solid-solution NTs, with the molar ratios of Mg^{2+}:Ni^{2+} = 0:2.0 (a_1, b, c, h_1, i_1); 0.5:1.5 (a_2, d, h_2, i_2); 1.0:1.0 (a_3, e, e_1, h_3, i_3); 1.5:0.5 (a_4, f, h_4, i_4); 2.0:0 (a_5, g, h_5, i_5). Composition: (a_1) $Ni_3Si_2O_5(OH)_4$ (JCPDS No. 49-1859); (a_2–a_4) $(Ni,Mg)_3Si_2O_5(OH)_4$ (JCPDS No. 25-0524); (a_5) $Mg_3Si_2O_5(OH)_4$ (JCPDS No. 52-1562). Mass of the samples within each vial (g): 0.900.

N_2 desorption isotherm using the Barrett–Joyner–Halenda (BJH) method. Qualitative analysis of the catalytic liquid phase was carried out on a gas chromatograph–mass spectrometer (GCMS-QP 2010 SE, Shimadzu, Japan), and the yield of the product biphenyl or 4-methylbiphenyl was determined with GC–MS measurements (Thermo Scientific DSQ, USA) by the selected ion monitoring method with iodobenzene included, using *n*-dodecane as the internal standard and ethanol as the solvent. The valence state of the element was determined by an X-ray photoelectron spectroscopy (XPS) microscope (ESCALAB250, Thermofisher, U.K., at 15 kV and 150 W). The intermediate liquid phase quenched during the first SM coupling reaction was concentrated by a rotary evaporator and monitored by an electron-spin resonance spectrometer (JES-FA200, JEOL, Japan), using the $(Ni,Mg)_3Si_2O_5(OH)_4$ (Mg^{2+}:Ni^{2+} = 1.0:1.0) NTs supported with or without sub-0.06 wt % Pd as the catalyst.

RESULTS AND DISCUSSION

1. Composition, Microstructure, and Optical Absorbance Property of the As-Synthesized NTs. Keeping the whole amount of Mg^{2+} and Ni^{2+} as 2.0 moles and tuning the molar ratios of Mg^{2+}:Ni^{2+} within the range of 0:2.0–2.0:0, the composition, morphology, color, and optical absorbance property of the hydrothermal products obtained at 210 °C for 24.0 h can also be tuned, as shown in Figure 1. When Mg^{2+}:Ni^{2+} = 0:2.0, the product was composed of the pure phase of $Ni_3Si_2O_5(OH)_4$ (JCPDS No. 49-1859) with high crystallinity (Figure 1a_1) and distinct tubular structure (Figure 1b,c), containing an inner diameter of 10–15 nm and an outer diameter of 20–30 nm, similar to the literature results.[24] The interplanar spacing of 0.753 nm detected from the legible lattice fringes along the axis direction of the as-obtained NTs was quite similar to that of the standard value for the (002) planes of monoclinic $Ni_3Si_2O_5(OH)_4$, indicating the axial direction of the $Ni_3Si_2O_5(OH)_4$ NTs parallel to the (002) planes (Figure 1c). As the molar ratios of Mg^{2+}:Ni^{2+} increased to 0.5:1.5 and 1.0:1.0, the product was constituted of the orthorhombic solid-solution phase of $(Ni,Mg)_3Si_2O_5(OH)_4$ (JCPDS No. 25-0524) with gradually decreased crystallinity (Figure 1a_2–a_3) and also a tubular structure (Figure 1d,e), bearing an inner diameter of 10–15 nm and an outer diameter of 20–30 nm. The interplanar spacings of 0.741 nm also confirmed the axial direction of the NTs along the (002) planes.

Compared with the previous NTs, when the molar ratio of Mg^{2+}:Ni^{2+} was 1.0:1.0, the as-obtained NTs (Figure 1e) were unstable under electron-beam irradiation even with a

dx.doi.org/10.1021/ic2024378 | *Inorg. Chem.* 2012, 51, 6020–6031

magnification as 40 K for a short time, resulting in porous structures (Figure 1e$_1$) and further failure to acquire the high-resolution transmission electron microscopy (HRTEM) image with legible lattice fringes. When the molar ratio of Mg^{2+}:Ni^{2+} was 1.5:0.5, the hydrothermal product was also the $(Ni,Mg)_3Si_2O_5(OH)_4$ phase with ordinary crystallinity (Figure 1a$_4$) and a tubular structure (Figure 1f), containing inner and outer diameters similar to the former ones. However, the detected interplanar spacings between lattice fringes along the axis of the NTs were slightly broadened to be 0.756 nm because of the successive increase of the molar ratio of Mg^{2+}:Ni^{2+}. With the molar ratio of Mg^{2+}:Ni^{2+} further increased to 2.0:0, the product was proven to be the pure phase of monoclinic $Mg_3Si_2O_5(OH)_4$ (JCPDS No. 52-1562) with relatively low crystallinity (Figure 1a$_5$) and also a tubular structure (Figure 1g).[25] The as-obtained NTs were also not stable under electron-beam irradiation and tended to be porous.

On the other hand, with the molar ratios of Mg^{2+}:Ni^{2+} increasing from 0:2.0 to 2.0:0, the color of the hydrothermally synthesized NTs changed from the original bottle green to bright green to light green and finally to white, as shown in Figure 1h. Meanwhile, different samples of the same mass (0.900 g) within the same sized vials demonstrated different heights because of the difference of the bulk density caused by the various porous structures of the NTs. The UV−vis diffuse-reflectance spectra (Figure 1i) showed that when the molar ratio of Mg^{2+}:Ni^{2+} = 0:2.0, 0.5:1.0, 1.0:1.0, and 1.5:0.5, the as-synthesized NTs exhibited distinct absorption within the near-UV region concentrated on the wavelength of 380 nm and also wider absorption within the visible and near-IR regions from 550 to 800 nm (Figure 1i$_1$−i$_4$). In accordance with the color changes of the NTs (Figure 1h$_1$−h$_4$), the UV−vis spectra also revealed some slight differences. When Mg^{2+}:Ni^{2+} was increased to 1.5:0.5, the absorption within the two regions tended to be weaker (Figure 1i$_4$). Notably, when Mg^{2+}:Ni^{2+} = 2.0:0, i.e., pure $Mg_3Si_2O_5(OH)_4$ NTs (Figure 1i$_5$), no distinct absorption was observed within the whole wavelength range tested, indicating the quasi-transparent characteristic of the $Mg_3Si_2O_5(OH)_4$ NTs within the UV−vis region.[26] Confirmed by the successive conversion of the X-ray diffraction (XRD) patterns, microstructures, colors, and UV−vis spectra, the compositions of the as-synthesized $(Ni_{1-x},Mg_x)_3Si_2O_5(OH)_4$ solid-solution NTs could thus be facilely tuned by altering the molar ratio of Mg^{2+}:Ni^{2+} from 0:2.0 to 2.0:0.

Figure 2 reveals the HAADF-STEM images and corresponding elemental mappings of the hydrothermally synthesized solid-solution NTs, with molar ratios of Mg^{2+}:Ni^{2+} = 0.5:1.5 (Figure 2a,a$_1$−a$_4$), 1.0:1.0 (Figure 2b,b$_1$−b$_4$), and 1.5:0.5 (Figure 2c,c$_1$−c$_4$). The dark-field STEM images clearly reconfirmed the tubular structures of the as-synthesized NTs, with different resolutions due to various crystallinities (Figure 2a−c). The higher the crystallinity of the NTs, the higher the resolution of the STEM image, in accordance with the XRD and TEM characterizations to some extent (Figure 1a$_2$−a$_4$,d−f). For all referred NTs, constitutional elements such as O, Mg, Si, and Ni were homogeneously dispersed within the bulk phase of the NTs. With the molar ratio of Mg^{2+}:Ni^{2+} increasing from 0.5:1.5 to 1.5:0.5, the orange mapping signals of Mg−K tended to be stronger (Figure 2a$_2$,b$_2$,c$_2$) and the green mapping signals of Ni−K became weaker (Figure 2a$_4$,b$_4$,c$_4$). However, although the $(Ni,Mg)_3Si_2O_5(OH)_4$ (Mg^{2+}:Ni^{2+} = 1.0:1.0) NTs have been loaded with sub-0.06 wt % Pd, neither the remarkable mapping signals of Pd−K nor those of Pd−L were detected for such a low loading (Figure 2b), which was below the detection limit of the apparatus. Apparently, the HAADF-STEM images and especially elemental mappings reconfirmed the successive conversion and facile tuning of the present $(Ni_{1-x},Mg_x)_3Si_2O_5(OH)_4$ solid-solution NTs, creating a tunable microenvironment containing different amounts of Ni and Mg.

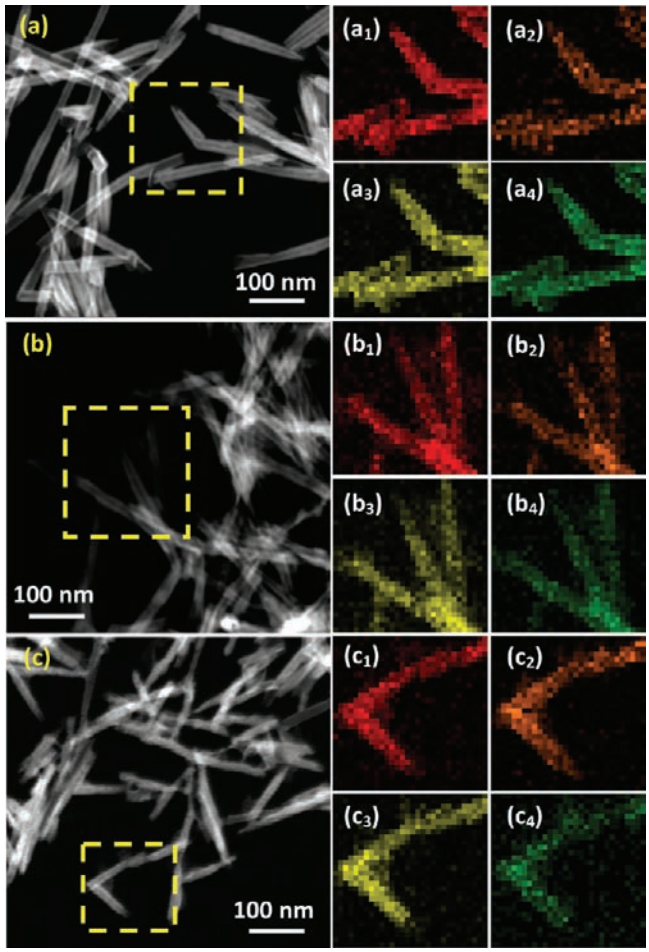

Figure 2. HAADF-STEM (a−c) images and corresponding elemental mappings (a$_1$−a$_4$, b$_1$−b$_4$, c$_1$−c$_4$) of the hydrothermally synthesized $(Ni_{1-x},Mg_x)_3Si_2O_5(OH)_4$ solid-solution NTs loaded without (a and c) and with (b) sub-0.06 wt % Pd before catalysis, with the molar ratios of Mg^{2+}:Ni^{2+} = 0.5:1.5 (a and a$_1$−a$_4$), 1.0:1.0 (b and b$_1$−b$_4$), and 1.5:0.5 (c and c$_1$−c$_4$). Elemental mapping: O−K (red, a$_1$, b$_1$, c$_1$); Mg−K (orange, a$_2$, b$_2$, c$_2$); Si−K (yellow, a$_3$, b$_3$, c$_3$); Ni−K (green, a$_4$, b$_4$, c$_4$).

2. Porous Structures of the $(Ni_{1-x},Mg_x)_3Si_2O_5(OH)_4$ NTs. Figure 3 shows the N_2 adsorption−desorption isotherms and corresponding pore diameter distribution of the NTs, and Table 1 further summarizes the porous structures of the NTs. The N_2 adsorption−desorption isotherms displayed a very similar type IV with an H3-type hysteresis loop at a high relative pressure (Figure 3a−e). The present hysteresis loops observed at high relative pressures were probably due to the textural mesoporosity among the randomly aggregated NTs. Meanwhile, the BJH desorption pore diameter distribution curves revealed a relatively broad distribution characteristic (Figure 3a$_1$−e$_1$), as confirmed in Table 1. All of the NTs had relatively large multipoint BET specific surface areas within the range of 100−210 m^2 g^{-1}. Particularly, the $(Ni,Mg)_3Si_2O_5(OH)_4$ (Mg^{2+}:Ni^{2+} = 1.0:1.0) NTs exhibited

dx.doi.org/10.1021/ic2024378 | Inorg. Chem. 2012, 51, 6020−6031

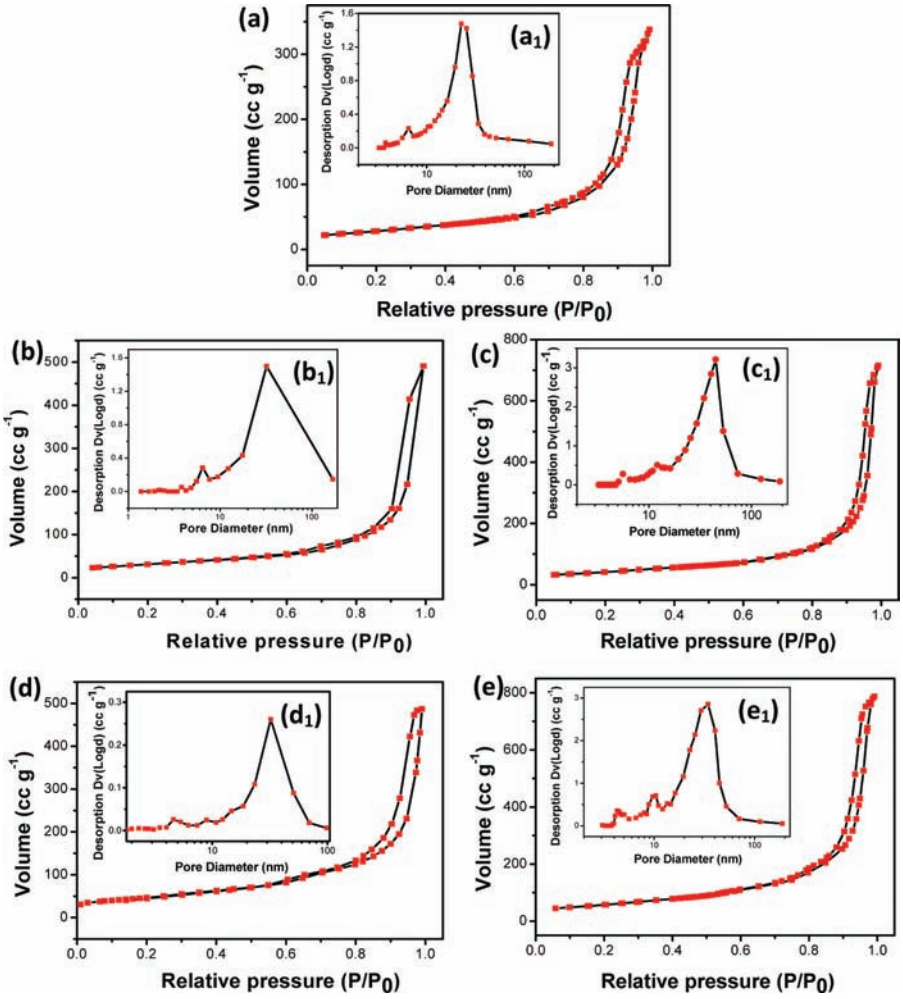

Figure 3. N_2 adsorption−desorption isotherms (a−e) and pore diameter distribution (a_1−e_1) of the hydrothermally synthesized $(Ni_{1-x}Mg_x)_3Si_2O_5(OH)_4$ solid-solution NTs, with molar ratios of Mg^{2+}:Ni^{2+} = 0:2.0 (a and a_1), 0.5:1.5 (b and b_1), 1.0:1.0 (c and c_1), 1.5:0.5 (d and d_1), and 2.0:0 (e and e_1).

Table 1. Porous Structures of the Hydrothermally Synthesized $(Ni_{1-x}Mg_x)_3Si_2O_5(OH)_4$ Solid-solution NTs, with Molar Ratios of Mg^{2+}:Ni^{2+} = 0:2.0 (a), 0.5:1.5 (b), 1.0:1.0 (c), 1.5:0.5 (d), and 2.0:0 (e)

	a	b	c	d	e
specific surface area (m^2 g^{-1})	101.5	113.8	152.3	165.47	209.1
total pore volume (cm^3 g^{-1})	0.523	0.754	1.107	0.757	1.217
average pore diameter (nm)	20.60	26.52	29.08	14.36	23.29
pore diameter distribution (nm)	3−7, 10−50	3−8, 10−100	5−7, 10−20, 20−100	4−6, 7.5−12, 14−70	4−6, 7−12, 15−90

not only large specific surface areas but also large total pore volumes and average pore diameters. The relatively large variation in the total pore volume between samples was probably associated with the difference of the stability or crystallinity of the NTs (Table 1). Mesopores with diameters within the range of 10−20 nm were due to the inner spaces of the tubular structures. In contrast, bigger mesopores larger than 20 nm or even macropores larger than 50 nm corresponded to those existing among the randomly stacked NTs. Obviously, the as-synthesized NTs exhibited some distinct characteristics, such as tunable compositions, relatively large specific surface area, total pore volumes, average pore diameters, and relatively broad pore diameter distribution. This indicated the as-synthesized $(Ni_{1-x}Mg_x)_3Si_2O_5(OH)_4$ NTs as potential ideal supports for the catalysts, especially nanocatalysts.

3. Single-Pass and Recycling Catalytic Performances of the $(Ni_{1-x}Mg_x)_3Si_2O_5(OH)_4$ NTs Supported by Sub-0.06 wt % Pd. The as-synthesized different types of NTs were loaded with sub-0.06 wt % Pd as the catalyst for the selected SM coupling reaction between iodobenzene and phenylboronic acid:

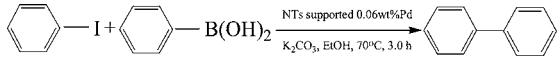

(5)

After the reduction of Pd^{2+} by ethanol, the liquid phase was separated by centrifugation and then enough $NaBH_4$ was added. As a result, no black precipitate was found, indicating the previously complete reduction of Pd^{2+} and also successful loading of Pd onto the NTs. Variation of the yield of biphenyl with different molar ratios of Mg^{2+}:Ni^{2+} for the hydrothermally

dx.doi.org/10.1021/ic2024378 | Inorg. Chem. 2012, 51, 6020−6031

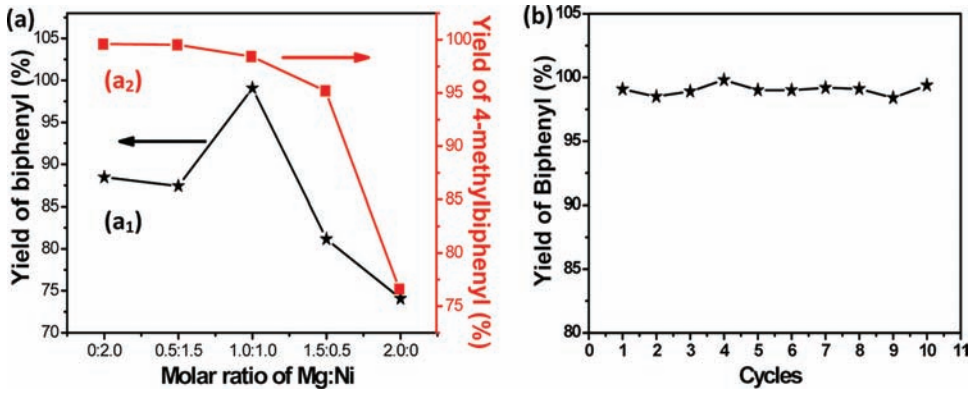

Figure 4. Single-pass (a) and recycling (b) catalytic performances of the as-synthesized $(Ni_{1-x},Mg_x)_3Si_2O_5(OH)_4$ NTs supported by sub-0.06 wt % Pd for the SM coupling reaction between iodobenzene (a_1 and b) or 4-iodotoluene (a_2) and phenylboronic acid, with molar ratios of Mg^{2+}:Ni^{2+} = 0:2.0−2.0:0 (a) and 1.0:1.0 (b).

synthesized NTs is shown in Figure 4a_1, with the same amount of NTs supported by Pd as the catalyst (denoted as the left Y axis). When Mg^{2+}:Ni^{2+} = 0:2.0, 0.5:1.5, 1.0:1.0, 1.5:0.5, and finally 2.0:0, the yield changed from 88.4% to 87.4% to 99.1% (peak value) and then significantly decreased to 81.2% and ultimately to 74.1%. Apparently, $(Ni,Mg)_3Si_2O_5(OH)_4$ (Mg^{2+}:Ni^{2+} = 1.0:1.0) NTs supported by sub-0.06 wt % Pd performed best as the catalyst for the selected coupling reaction between iodobenzene and phenylboronic acid.

To further evaluate the catalytic activity of the hydrothermally synthesized NTs supported by sub-0.06 wt % Pd, a second SM coupling reaction between 4-iodotoluene and phenylboronic acid was also performed as follows:

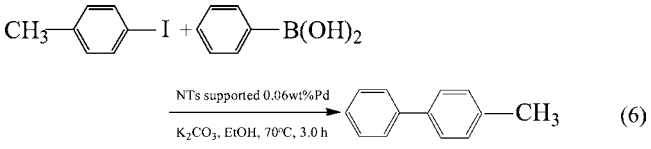

(6)

Figure 4a_2 indicates the yield of 4-methylbiphenyl (denoted as the right Y axis). When the molar ratio of Mg^{2+}:Ni^{2+} increased from 0:2.0 to 0.5:1.5, 1.0:1.0, 1.5:0.5, and finally 2.0:0, the yield gradually decreased from 99.6% to 99.5%, 98.4%, 95.2%, and finally 76.6%, respectively. Using the same amounts of the NTs supported by sub-0.06 wt % Pd as the catalyst, the monotonic alteration of the yield with the molar ratios of Mg^{2+}:Ni^{2+} for the second SM coupling reaction was slightly different from that for the first one, probably because of the various molar ratios of Mg^{2+}:Ni^{2+}, microstructures of the NTs, and also the intrinsic characteristics of the selected reactions. Expectedly, $(Ni,Mg)_3Si_2O_5(OH)_4$ (Mg^{2+}:Ni^{2+} = 1.0:1.0) supported by sub-0.06 wt % Pd could be utilized as a high-efficiency catalyst for the selected SM coupling reactions, something to do with the high specific surface area and total pore volume, which, however, seemed not to be the crucial factor, taking the ill catalytic performances of the $Mg_3Si_2O_5(OH)_4$ NTs supported by sub-0.06 wt % Pd into consideration (Table 1).

To investigate the recycling catalytic performance, the solid phase, i.e., $(Ni,Mg)_3Si_2O_5(OH)_4$ (Mg^{2+}:Ni^{2+} = 1.0:1.0) NTs supported by sub-0.06 wt % Pd catalyst, was recovered after the single-pass first SM coupling reaction and employed for the next new catalysis. As shown in Figure 4b, although after each cycle of catalysis the solid catalyst was separated by centrifugation, washed with DI water, separated again, then washed with ethanol, and finally participated in the next loop of catalysis, the yield of biphenyl did not drop significantly. As a matter of fact, even though the original 0.2 g of $(Ni,Mg)_3Si_2O_5(OH)_4$ (Mg^{2+}:Ni^{2+} = 1.0:1.0) NTs supported by sub-0.06 wt % Pd was collected as 0.10 g after the 9th cycle and 0.09 g after 10th cycle of catalysis, the yield of biphenyl fluctuated within the range of 98.5−99.4%, during the 10 cycles of catalysis.

The specific actual amount of Pd loading on the $(Ni,Mg)_3Si_2O_5(OH)_4$ (Mg^{2+}:Ni^{2+} = 1.0:1.0) NTs was further determined by ICP-MS, and the details of the sample preparation as well as the analytical results were also given, as shown in Table S1 (Supporting Information, SI). The actual Pd amounts loaded on the $(Ni,Mg)_3Si_2O_5(OH)_4$ (Mg^{2+}:Ni^{2+} = 1.0:1.0) NTs before the 1st cycle and after the 10th cycle of catalysis were 0.0449 and 0.0447 wt %, respectively. Thus, on the one hand, the specific Pd loading of the $(Ni,Mg)_3Si_2O_5(OH)_4$ (Mg^{2+}:Ni^{2+} = 1.0:1.0) NTs supported by sub-0.06 wt % Pd with high-efficiency single-pass and recycling catalytic performances was determined as 0.045 wt %. On the other hand, the Pd loading on the NTs almost did not change after 10 cycles of catalysis, implying no or neglectable Pd leaching in the selected catalysis using the present NTs supported by a trace amount of Pd as the catalyst. Typical GC−MS spectra of the liquid phase derived from the 1st, 4th, 7th, and 10th cycles of catalysis are shown in Figures S1−S4 (SI), respectively. It was notable that, although the collected solid catalyst gradually became less and less during the past 10 cycles of catalysis predominately owing to the loss originating from the separation and transformation, the yield still remained relatively stable or, strictly speaking, fluctuated slightly. In combination with the ICP-MS results (Table S1 in the SI), it was believed that there was just very slight leaching of Pd during the catalytic process or, in other words, almost all of the Pd species have redeposited onto the solid $(Ni,Mg)_3Si_2O_5(OH)_4$ (Mg^{2+}:Ni^{2+} = 1.0:1.0) NTs after catalysis.

The unexpected good recycling performance revealed that the SM reaction between iodobenzene and phenylboronic acid might have reached or passed the terminal point within the designated time, or put another way, there might also exist some space for reducing the Pd loading to achieve the present yield within the present time. Thus, specific control experiments were designed to further ascertain the robust high-efficiency catalyst. Figure S5 (SI) shows the GC−MS spectra of

dx.doi.org/10.1021/ic2024378 | Inorg. Chem. 2012, 51, 6020−6031

Table 2. Comparison of the Pd Catalyst Supported on the Present $(Ni,Mg)_3Si_2O_5(OH)_4$ (Mg^{2+}:Ni^{2+} = 1.0:1.0) NTs and Other Supports, for the Selected SM Coupling Reaction between Iodobenzene and Phenylboronic Acid

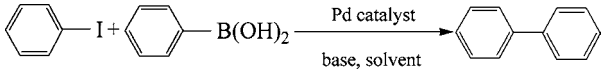

entry	catalyst support	Pd loading (wt %)[a]	Pd/iodobenzene (mol %)	reaction conditions solvent/base/temperature/time	no. of cycles	average isolated yield (%)[b]	ref
1	silica-APTS	2.3	1.0	DMA/K_2CO_3/100 °C/2 h[c]	15	95.5 (99–93)	27
2	MgO	10.53	0.5	H_2O/K_2CO_3/RT/5–6 h	5	(95–92)	55
3	DOPA-pine- Fe_2O_3	7.26	3.4	DMF–H_2O/K_2CO_3/100 °C/10 min[d]	5	95 (97–94)	56
4	MWCNT	3	0.28	MeOH/NaOAc/reflux/2 h	nr	95	28
5	PVC-DETA	6.4	0.25	DMF–H_2O/$NaHCO_3$/90 °C/4–10 h	8	96 (100–93)[e]	29
6	PDrum	6.04	nr	toluene/K_2CO_3/reflux/4 h	10	95 (95)	30
7	MCM41	5.53	0.6	dioxane/K_2CO_3/80 °C/2 h	10	96 (96)	31
8	TGAP	1.0	0.94	dioxane–H_2O/K_2CO_3/90 °C/24 h	5	98.5 (99–98)[e]	32
9	NHC	1.17	1.0	DMF–H_2O/Na_2CO_3/50 °C/1 h	10	94 (95–92)	57
10	PNIPAM	5.50	0.2[f]	DMA–heptane–H_2O/TEA/95 °C/20 h	5	65 (92–32)	33
11	$(Ni,Mg)_3Si_2O_5(OH)_4$ NTs	0.045[g]	0.11	EtOH/K_2CO_3/70 °C/3 h	10	99 (99.4–98.4)[e]	this work

[a]Percentage data showing wt % Pd loading when available; data in parentheses indicate mol % Pd used. [b]Data in parentheses showing the range of yields. [c]Under a nitrogen atmosphere. [d]Under microwave irradiation. [e]GC yield. [f]Molar ratio of Pd to support. [g]Actual amount of Pd loaded on the NTs, with 0.022 wt % Pd leading to a yield of 96.9% in single-pass catalysis.

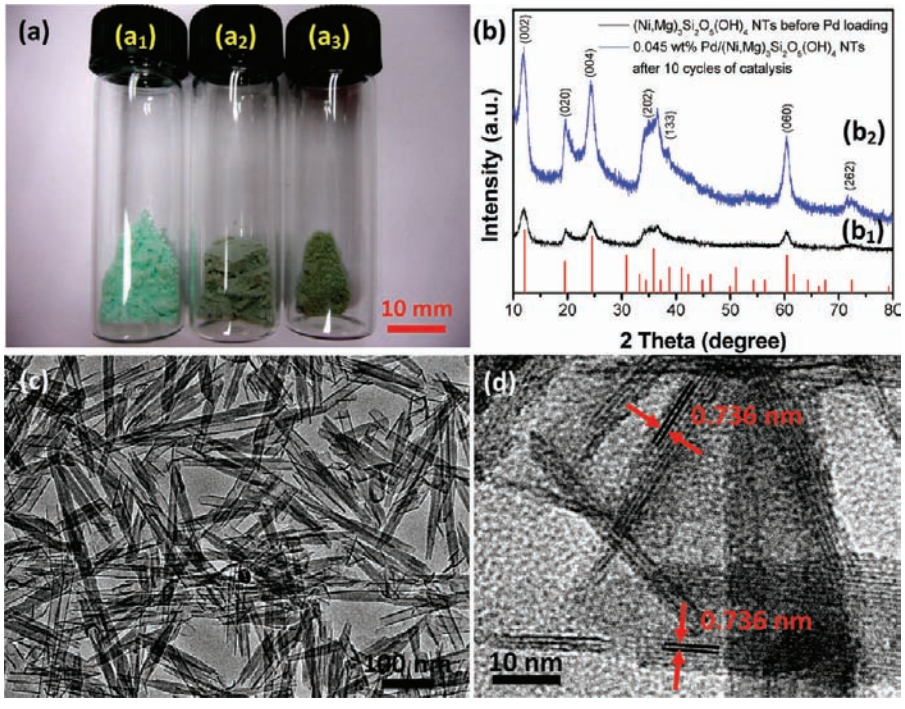

Figure 5. Digital picture (a), XRD patterns (b), and TEM images (c and d) of the $(Ni,Mg)_3Si_2O_5(OH)_4$ (Mg^{2+}:Ni^{2+} = 1.0:1.0) NTs before (a_1 and b_1) and after (a_2) 0.045 wt % Pd loading and also those after 10 cycles of catalysis (a_3, b_2, c, and d), with a molar ratio of Mg^{2+}:Ni^{2+} = 1.0:1.0. Vertical line in (b): standard pattern for $(Ni,Mg)_3Si_2O_5(OH)_4$ (JCPDS No. 25-0524).

the liquid product phase derived from the specifically designed reaction system using $(Ni,Mg)_3Si_2O_5(OH)_4$ (molar ratio of Mg^{2+}:Ni^{2+}= 1.0:1.0) NTs loaded with 0.022 wt % Pd as the catalyst. Suprisingly, even with half of the Pd loading as employed previously, no significant amount of residual iodobenzene was detected, and the yield was quite satisfactory as 96.9%. Nevertheless, the blank test indicated that when bare $(Ni,Mg)_3Si_2O_5(OH)_4$ (molar ratio of Mg^{2+}:Ni^{2+} = 1.0:1.0) NTs without Pd loading as the catalyst were utilized, no remarkable biphenyl was detected and the yield was neglectable as less than 0.15% (Figure S6 in the SI). Consequently, on the one hand, the presence of an appropriate amount of Pd was absolutely necessary, but, on the other hand, such a low loading as 0.022 wt % Pd on the present $(Ni,Mg)_3Si_2O_5(OH)_4$ (molar ratio of Mg^{2+}:Ni^{2+} = 1.0:1.0) NTs exhibited a satisfactory high yield for the selected single-pass SM coupling reaction.

The catalytic performance of the $(Ni,Mg)_3Si_2O_5(OH)_4$ (Mg^{2+}:Ni^{2+} = 1.0:1.0) NTs supported by 0.045 wt % Pd is further summarized in Table 2, based on a comparison with the reported results using supported Pd for the same SM coupling reaction. As can be seen, compared with those immobilized on inorganic materials,[27,28] the necessary Pd loading (correspond-

dx.doi.org/10.1021/ic2024378 | Inorg. Chem. 2012, 51, 6020–6031

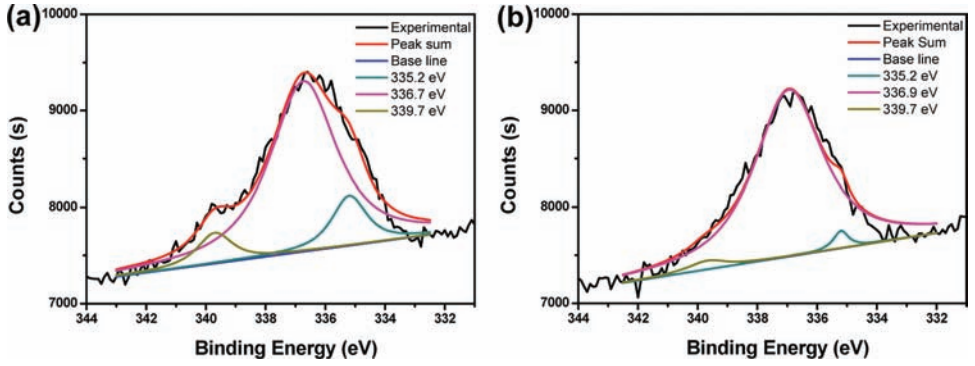

Figure 6. Core-level Pd 3d XPS spectra taken from the $(Ni,Mg)_3Si_2O_5(OH)_4$ (Mg^{2+}:Ni^{2+} = 1.0:1.0) NTs supported by 0.045 wt % Pd before the 1st cycle (a) and after the 10th cycle (b) of catalysis, with a molar ratio of Mg^{2+}:Ni^{2+} = 1.0:1.0. BEs of 335.2 and 339.7 eV: Pd $3d_{5/2}$ and Pd $3d_{3/2}$ for metallic Pd, respectively. BEs of 336.7 and 336.9 eV: Pd $3d_{5/2}$ for Pd^{2+} in PdO.

ing to the support) and required Pd (corresponding to iodobenzene) were within the ranges of 2.3−10.53 wt % and 0.28−3.4 mol %, respectively. The referred inorganics supported by Pd NPs were generally recycled 5−15 times, with an average isolated yield of ca. 95%. For polymer-supported Pd NPs,[29,30] the amounts of Pd loaded and employed were 6.04−6.4 wt % and 0.25 mol %, respectively, with the recycles of 8−10 times and an average yield of 95−96%. In addition to Pd NPs, Pd complexes were also immobilized on a mesoporous silicate molecular sieve MCM-41[31] and so on.[32,33] In contrast with the Pd NPs or complexes immobilized on the above-described supports, the as-synthesized $(Ni,Mg)_3Si_2O_5(OH)_4$ (Mg^{2+}:Ni^{2+} = 1.0:1.0) NTs in this work only contained 0.045 wt % Pd (corresponding to the supports) and 0.11 mol % (corresponding to iodobenzene) but could be recycled at least 10 times with an average GC yield of 99% (Table 2, entry 11). It was clear that both the amount of Pd loaded and that employed versus iodobenzene were much lower than those reported in the literature. Moreover, although each referenced case could reach higher yield, when the time was prolonged long enough, the present work indicated the $(Ni,Mg)_3Si_2O_5(OH)_4$ (Mg^{2+}:Ni^{2+} = 1.0:1.0) NTs supported by 0.045 wt % Pd as a robust high-efficiency catalyst for the traditional SM coupling reaction with excellent recycling catalytic performance, within the present short time.

4. Further Characterization of the Trace Pd Supported on $(Ni,Mg)_3Si_2O_5(OH)_4$ NTs. To probe the robust catalytic performance of the present supported trace Pd catalyst, the trace amount of Pd supported on the $(Ni,Mg)_3Si_2O_5(OH)_4$ (Mg^{2+}:Ni^{2+} = 1.0:1.0) NTs was further characterized. Figure 5 shows the digital picture, XRD patterns, and TEM images of the $(Ni,Mg)_3Si_2O_5(OH)_4$ NTs before and after 0.045 wt % Pd loading and also those after 10 cycles of catalysis. The color of the $(Ni,Mg)_3Si_2O_5(OH)_4$ (Mg^{2+}:Ni^{2+} = 1.0:1.0) NTs changed from bright green (Figure $5a_1$, bare NTs) to dark green (Figure $5a_2$, after 0.045 wt % Pd loading) and remained almost unchanged after 10 cycles of catalysis (Figure $5a_3$). Compared with those original NTs before Pd loading (Figure $5b_1$), the $(Ni,Mg)_3Si_2O_5(OH)_4$ (Mg^{2+}:Ni^{2+} = 1.0:1.0) NTs supported by 0.045 wt % Pd exhibited much higher crystallinity after 10 cycles of catalysis (Figure $5b_2$), due to a series of SM coupling reactions at 70 °C for 3.0 h each time. As can be seen, the trace loading of 0.045 wt % Pd did not change the crystal phase of the hydrothermally synthesized NTs. Notably, however, no diffraction peak of Pd was detected, owing to the low loading amount, which was far below the detection limit of XRD. This was quite different from the XRD pattern recorded from 7.0 wt % Pd/CNT.[34]

On the other hand, the TEM (Figure 5c) and HRTEM (Figure 5d) images reconfirmed the well-preserved tubular structure and greatly improved crystallinity, without significant mesopores within the walls observed after long-time electron-beam irradiation, compared with the unstable ones before Pd loading (Figure 1e). The legible lattice fringes bearing interplanar spacings of 0.736 nm also confirmed the axial direction of the NTs parallel to the (002) planes. This revealed the excellent hydrothermal stability of the as-synthesized $(Ni,Mg)_3Si_2O_5(OH)_4$ (Mg^{2+}:Ni^{2+} = 1.0:1.0) NTs without destruction after 10 cycles of high-efficiency catalysis under the base conditions, which were initially derived from an environmentally rich base during hydrothermal synthesis. Unfortunately, an attempt to seek the Pd NPs by TEM and HRTEM failed, although tiny Pd NPs could grow bigger during the series of catalysis because of the well-known Ostwald ripening mechanism.[35] As reported, Pd NPs also failed to be found within even 0.4 wt % $Pd(NH_3)_4Cl_2$/USY zeolite by TEM and HRTEM,[23] not to mention the present 0.045 wt % Pd loading.

XPS spectra were recorded on the $(Ni,Mg)_3Si_2O_5(OH)_4$ NTs (Mg^{2+}:Ni^{2+} = 1.0:1.0) supported by 0.045 wt % Pd collected before the 1st cycle and after the 10th cycle of catalysis, as shown in Figures S7 (SI) and 6. Spectra of Ni 2p (Figure S7a), Mg 2p (Figure S7b), Si 2p (Figure S7c), and O 1s (Figure S7d) reconfirmed the constitutional elements within the as-synthesized $(Ni,Mg)_3Si_2O_5(OH)_4$ NTs, in accordance the elemental mapping (Figure 3) and XRD (Figure 5b) results. The XPS spectra from the Pd 3d core-level region were also captured on the NTs supported by 0.045 wt % Pd in both cases, and the asymmetric experimental photoelectron lines could also be deconvoluted (Figure 6). The binding energies (BEs) of 335.2 and 339.7 eV corresponded with the Pd $3d_{5/2}$ and Pd $3d_{3/2}$ peaks of the metallic Pd, respectively, in good agreement with the literature results.[36] The BEs of 336.7 and 336.9 eV were more likely assigned to the Pd $3d_{5/2}$ peak for Pd^{2+} in PdO.[36,37] Takasu and co-workers reported that Pd NPs of 1.6 nm diameter gave rise to a BE of 336.6 eV,[38] very similar to 336.7 and 336.9 eV in the present case. Thus, both phases of PdO and metallic Pd NPs, or clusters, might have contributions to the BE of 336.7 and 336.9 eV. Probably, the formation of the PdO phase was attributed to oxidation of the metallic Pd cluster phase during separation of the product and transfer of the recovered solid-solution NT phase between the various cycles

dx.doi.org/10.1021/ic2024378 | Inorg. Chem. 2012, 51, 6020−6031

of catalysis, owing to the intrinsic high activity of the clusters themselves.

To further understand the robust high-efficiency $(Ni,Mg)_3Si_2O_5(OH)_4$ (Mg^{2+}:Ni^{2+} = 1.0:1.0) NTs supported by trace Pd clusters and a possible catalytic mechanism, the electron-spin resonance (ESR) spectra were recorded from the intermediate liquid phase quenched during the first SM coupling reaction, using the as-synthesized NTs supported by 0.045 wt % Pd as the catalyst and also bare ones without Pd loading for comparison. As shown in Figure 7, the liquid

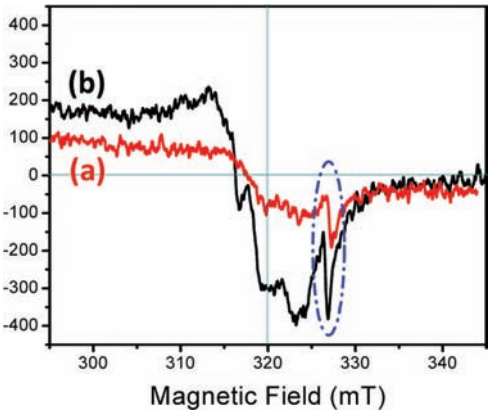

Figure 7. ESR spectra of the liquid phase quenched during the SM coupling reaction, with $(Ni,Mg)_3Si_2O_5(OH)_4$ (Mg^{2+}:Ni^{2+} = 1.0:1.0) NTs supported by 0.045 wt % Pd (a) and bare NTs without Pd loading (b) as the catalyst.

quenched from the $(Ni,Mg)_3Si_2O_5(OH)_4$ (Mg^{2+}:Ni^{2+} = 1.0:1.0) NTs supported by a 0.045 wt % Pd system exhibited a significant resonance peak in the magnetic field range of 326–330 mT (Figure 7a). However, bare NTs without Pd loading (Figure 7b) also demonstrated a significant resonance peak at the same magnetic field range, denoted as the blue dash-dotted elliptical region. This implied the absence of a Pd single-electron resonance, indicating the absence of the odd-valence Pd species such as Pd^+ or Pd^{3+} within the quenched intermediate catalytic system.

Thus, the XPS Pd 3d spectra directly and macroscopically confirmed the existence of Pd species loaded on the NTs, in combination with the ICP-MS results (Table S1 in the SI). Nevertheless, owing to the low Pd loading (0.045 wt %) on the unstable NTs (Mg^{2+}:Ni^{2+} = 1.0:1.0), the Pd species was neither successfully detected by XRD nor straightforward captured by TEM, elemental mapping, and HRTEM. Taking the rapid reduction during the trace Pd loading within the EtOH–water phase into account, it was assumed that Pd clusters should have been formed after reduction and further highly dispersed onto the $(Ni,Mg)_3Si_2O_5(OH)_4$ NTs (Mg^{2+}:Ni^{2+} = 1.0:1.0). As a consequence, the inherent extremely small size and surface effect contributed to the instability and high activity of the Pd clusters, which was also found in some other Pd-catalyzed reactions.[22,23,39−41] This was quite similar to the gold particles highly dispersed on the ZrO_2 surface at a low loading level of 0.01–0.08 wt %.[42,43]

On the basis of the above analysis, it was rational to speculate that each Pd atom was a catalytic active site. Thus, as shown in Table S2 (SI), using $(Ni,Mg)_3Si_2O_5(OH)_4$ (Mg^{2+}:Ni^{2+} = 1.0:1.0) NTs supported by 0.045 wt % Pd as the catalyst, the turnover numbers (TONs)[44] for the 1st and 10th cycles of the SM reaction between iodobenzene and phenylboronic acid were assessed as 1162 and 2347, respectively; the corresponding turnover frequencies (TOFs)[44] were also assessed as 0.1076 and 0.2174 s^{-1}, respectively. Owing to the above assumption, the assessed TONs and TOFs were believed to be somehow smaller than the authentic values.

5. Possible Catalytic Mechanism of the $(Ni,Mg)_3Si_2O_5(OH)_4$ NTs Supported by 0.045 wt % Pd.

Variation of the Pd concentration during catalysis was monitored so as to confirm migration of the Pd species. The GC yield and ICP-MS results are listed in Table S3 (SI), and the corresponding GC spectra of some extended control experiments are shown in Figure S8 (SI). As can be seen, for the quenched system (Table S3, entry 1, and Figure S8a in the SI), the naturally cooled system (Table S3, entry 2, and Figure S8b in the SI) exhibited higher yield owing to the proceeding reaction during the cooling process. Meanwhile, the Pd concentration of the cooled system was determined as 43.6 ng mL^{-1} (i.e., ppb), much higher than that of the quenched one (14.8 ng mL^{-1}). It implied that the rapid quenching promoted redeposition of active Pd species to the solid-solution NT phase. In addition, the coherent reaction without in-between interruption (Table S3, entry 3, in the SI) exhibited a final high yield (99.1%) and a low Pd concentration (23.6 ng mL^{-1}, ~0.02 ppm). Notably, the Pd/C-catalyzed SM coupling reaction exhibited a significant Pd leaching of 3 ppm in the organic dimethylacetimide (DMA)/triethylamine (TEA) solvents after 4.0 h of reaction;[45] 1.0 wt % Pd/TGAP revealed a relatively low Pd leaching of less than 0.4 ppm in the reaction system;[32] 2.3 wt % Pd/silica-APTS demonstrated a lower Pd leaching of less than 0.17 ppm.[27] Crudden and co-workers reported an excellent Pd catalyst supported on mercaptopropyl-modified mesoporous silica, which has been recognized as one of the best catalytic Pd materials with lowest leaching (72–3 ppb in 2.5 mL of solvent; average 242 ng for 4 runs).[40,46] Hoshiya and co-workers provided a low-releasing Pd catalyst supported on sulfur-modified gold via treatment with a piranha solution (12.7–6.3 ppb in 3 mL of solvent; average 26 ng for 10 runs).[47] In contrast, the present NTs supported by 0.045 wt % Pd exhibited a low Pd concentration of 0.0236 ppm (23.6 ppb) in 7.5 mL of solvent (177 ng) after the first run. Because Pd leaching decreased significantly from the second run and tended lower and lower in the subsequent recycling performances,[32,48] the overall Pd dissociated into the present 10 cycles of catalysis was estimated at an extremely low level, lower than that of the Pd material provided by Crudden et al.[40,46] and also comparable to that presented by Hoshiya et al.[47]

On the other hand, a higher concentration of Pd species within the liquid phase propelled the formation of product biphenyl. In addition, the liquid phase derived from either the quenched (Figure S8c in the SI) or cooled (Figure S8d in the SI) system after centrifugation could further react continuously itself when reheated to 70 °C for another 4.0 h, resulting in a higher yield of biphenyl, without the aid of solid-solution NTs supported by Pd. This definitely ascertained the presence of Pd species within the liquid product phase, in good agreement with the ICP-MS results. Comparatively, the fresh reaction system was also catalyzed by the sedimental phase of the quenched system at 70 °C for 4.0 h (Figure S8e in the SI), giving rise to a quite high yield (ca. 96%), implying more active Pd species redeposited onto the solid-solution NT phase after quenching. This test was similar to the classical hot filtration or centrifugation test,[15,49] to some extent. As reported, however,

dx.doi.org/10.1021/ic2024378 | Inorg. Chem. 2012, 51, 6020–6031

the hot filtration test is probably useful if the bulk metal catalyst, rather than the nanocluster catalyst, is responsible for catalysis.[49] Similarly, for the nanocluster-participated catalysis, the centrifugation test could hardly achieve an ideal quantitative separation of the sediment and supernatant, and, as a consequence, both of them will probably have some residual catalytic activity. Especially, the centrifugation test will not work when the reaction is catalyzed by a low concentration of highly active nanoclusters because no visible sediment will form.[49]

To gain deeper insight into the catalytic active species, the classical mercury poisoning experiment was carried out, which has been well established for distinguishing heterogeneous from homogeneous catalysis, with the aid of a requisite control experiment.[49,50] As shown in Figure S9 (SI), the GC spectra of the liquid phase acquired from the quenched system when catalysis proceeded for 15.0 min (Figure S9a in the SI) and that recovered for catalysis for another 2.0 h and 45.0 min after the mercury poisoning (Figure S9b in the SI) exhibited the same characteristics with the same yield of the product biphenyl. This indicated that the addition of excess mercury (125.2 mg; molar ratio of Hg^0 to Pd ~ 1480) has completely suppressed the SM cross-coupling reaction between iodobenzene and phenylboronic acid. As reported, the coupling of iodoarenes could be homogeneously catalyzed by Pd ultratraces at a temperature higher than 100 °C, by using palladacycles as catalysts.[51,52] However, in these nice researches, carefully designed ligands are needed to ensure high reactivity of these catalysts. In our work, no special ligands are present during the catalysis process, which greatly lowers the possibility of homogeneous catalysis by a trace amount of Pd released to the organic solution. Thus, taking the present mercury poisoning test and also the previous SM cross-coupling reaction (Figure 4) without mercury poisoning performed at 70 °C into consideration, the $(Ni,Mg)_3Si_2O_5(OH)_4$ (Mg^{2+}:Ni^{2+} = 1.0:1.0) NTs supported by 0.045 wt % Pd catalyst exhibited distinct genuine heterogeneous catalytic nature. Objectively, the Pd concentrations of the intermediate and final product liquid phase detected (Table S3 in the SI) were probably due to the release of Pd nanoclusters dissociated from the bulk NT phase, different from those of leached soluble Pd species in other homogeneous catalyses.

On the basis of the almost unchanged 0.045 wt % of the actual Pd loading amount on the NTs before the 1st cycle and after the 10th cycle of catalysis (Table S1 in the SI), centrifugation-like (Table S3 and Figure S8 in the SI), and especially the mercury poisoning (Figure S9 in the SI) experimental results, the detected Pd species within the intermediate supernatant derived from centrifugation (Table S3 and Figure S8 in the SI) were firmly believed to be the solid Pd nanoclusters dissociated from the bulk NTs during catalysis performed at elevated temperature under vigorous magnetic stirring rather than the soluble or leached Pd species. The dissociated Pd nanoclusters within the supernatant contributed to further catalysis after centrifugation. Moreover, the SM cross-coupling reaction took place on the surfaces of the Pd nanoclusters rather than the homogeneous solution phase, definitely demonstrating the genuine heterogeneous catalytic characteristic. The present active Pd nanoclusters were different from the leached Pd species in the liquid phase, which have become accepted in Heck and some other coupling reactions.[8,53] Because absolute leaching of soluble Pd species could not be excluded thoroughly and the Pd ultratraces released into the organic solution could catalyze the coupling of iodoarenes in due course,[51,52] the hypotheses of the possible effect of the leached soluble Pd ultratraces on the present catalysis could not be discarded entirely, which, however, was somehow believed to be inappreciable and thus neglectable.

Similar to the catalytic cycle for the Pd/C-catalyzed SM coupling reaction,[54] the possible catalytic cycle of the Pd/$(Ni,Mg)_3Si_2O_5(OH)_4$-catalyzed SM coupling reaction, which took place on the surfaces of the Pd nanoclusters deposited on the solid-solution NTs, could thus be depicted based on the above results, as shown in Scheme 1. The cycle consisted of five

Scheme 1. Possible Catalytic Cycle of the Pd/$(Ni,Mg)_3Si_2O_5(OH)_4$-Catalyzed SM Coupling Reaction Taken Place on the Surfaces of the Pd Clusters Deposited on the Solid-Solution NTs: (i) Oxidative Addition and Resultant Pd Leaching; (ii) Metathesis due to the Addition of Hydroxide Ion OH^- Originating from Dissociation of the Base K_2CO_3; (iii) Transmetalation Owing to the Arylborate Activation; (iv) Reductive Elimination Leading to Pd Clusters and Product Containing a Trace Amount of Leached Pd; (v) Precipitation of Pd Clusters onto the $(Ni,Mg)_3Si_2O_5(OH)_4$ NTs, Partially Oxidized to PdO due to High Activity

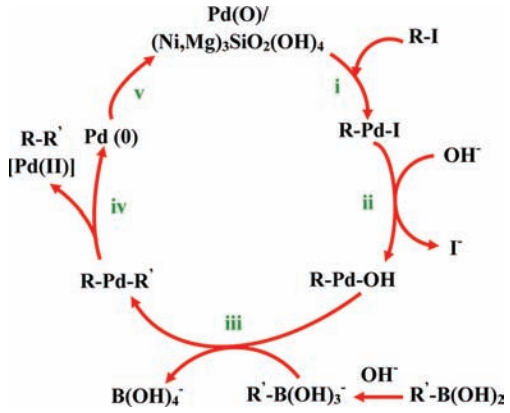

main steps: oxidative addition and resultant Pd leaching (i), metathesis due to the addition of hydroxide ion OH^- originating from dissociation of the base K_2CO_3 (ii), transmetalation owing to arylborate activation (iii), reductive elimination leading to Pd nanoclusters and product containing very trace amounts of leached Pd (iv), and precipitation of Pd nanoclusters onto the $(Ni,Mg)_3Si_2O_5(OH)_4$ NTs with probably and partially oxidized PdO due to high activity (v). It was clear that the base played a key role in the whole catalytic cycle within the above metathesis (ii) and transmetalation (iii), which gave rise to R−Pd−OH and tetrahedral boronate $B(OH)_4^-$, respectively. Of note was that, however, beyond the figured seemingly closed catalytic cycle, the separation of liquid product containing a very trace amount of leached Pd and transfer of recovered solid-solution NTs supported by Pd between various catalytic cycles would lead to Pd loss out of the cycle to some extent. The physical separation and transfer were responsible for the overall Pd loss, taking the almost consistent Pd loading amount on the $(Ni,Mg)_3Si_2O_5(OH)_4$ (Mg^{2+}:Ni^{2+} = 1.0:1.0) NTs before the 1st cycle and after the 10th cycle of catalysis into account (Table S1 in the SI).

As for the present robust high-efficiency $(Ni,Mg)_3Si_2O_5(OH)_4$ NTs supported by 0.045 wt % Pd catalyst, three more aspects should also be taken into

dx.doi.org/10.1021/ic2024378 | Inorg. Chem. 2012, 51, 6020−6031

consideration. First, high-activity Pd nanoclusters could be oxidized to PdO (Figure 6) clusters during the separation of liquid product and transfer of recovered solid-solution NTs supported by a catalyst. Because Pd^{II} is prone to leaching,[8] the PdO clusters might promote the subsequent metathesis, compared with pure Pd nanocluster phase. Second, the specific unstable $(Ni,Mg)_3Si_2O_5(OH)_4$ (Mg^{2+}:Ni^{2+} = 1.0:1.0) NTs contained multitudes of dislocations, defaults, and terraces, which could serve as particularly ideal reservoirs for the reduction formation and in situ deposition of the newly formed tiny Pd nanoclusters of different sizes, and this could also account for the extremely low or even neglectable Pd leaching level during the 10 cycles of catalysis. Third, extensive investigation revealed that the present $(Ni,Mg)_3Si_2O_5(OH)_4$ (Mg^{2+}:Ni^{2+} = 1.0:1.0) NTs supported by 0.045 wt % Pd did not perform well for the SM cross-coupling reaction between the more challenging substrates, e.g., the nonactivated aryl bromides, with phenylboronic acid. To get the relatively satisfactory conversion and yield, higher yield of the product, higher Pd loading, and more NTs supported by the Pd catalyst, higher temperature and longer time were necessary. Finally, because low-crystallinity $Mg_3Si_2O_5(OH)_4$ NTs (with also high specific surface area and analogous tubular structure; Figure 1g) supported by the same amount of Pd exhibited relatively low yield (Figure 4a), the possible synergistic effect of Ni−Mg for the $(Ni,Mg)_3Si_2O_5(OH)_4$ (Mg^{2+}:Ni^{2+} = 1.0:1.0) NTs supported by Pd should also contribute to the corresponding high yield, excellent recycling catalytic performance, and extremely low Pd release, which, however, needed further investigation and deeper understanding.

CONCLUSION

In summary, $(Ni_{1-x}Mg_x)_3Si_2O_5(OH)_4$ solid-solution NTs with tunable compositions were synthesized via a facile hydrothermal route at 210 °C for 24.0 h, by tuning the molar ratio of Mg^{2+} to Ni^{2+} within the range of 0:2.0 to 2.0:0. The as-synthesized NTs were loaded with 0.045 wt % Pd for the SM coupling reactions between iodobenzene or 4-iodotoluene and phenylboronic acid. $(Ni,Mg)_3Si_2O_5(OH)_4$ (Mg^{2+}:Ni^{2+} = 1.0:1.0) NTs supported by 0.045 wt % Pd promoted the iodobenzene-participated coupling reaction with a high yield of >99%, an excellent recycling catalytic performance during 10 cycles of catalysis with yields of ∼99%, and also an extremely low Pd releasing level of ∼0.02 ppm. After 10 cycles of catalysis, $(Ni,Mg)_3Si_2O_5(OH)_4$ (Mg^{2+}:Ni^{2+} = 1.0:1.0) NTs exhibited well-defined tubular structures and higher crystallinity. The almost consistent actual Pd loading amount on the NTs before the 1st cycle and after the 10th cycle of catalysis and Pd 3d XPS spectra directly confirmed the robust stable existence of Pd and partially oxidized PdO clusters supported on the NTs. In addition, $(Ni,Mg)_3Si_2O_5(OH)_4$ NTs supported by 0.022 wt % Pd could also catalyze the SM coupling of iodobenzene and phenylboronic acid with a satisfactory yield of ∼97%. High-activity Pd and PdO clusters, special $(Ni,Mg)_3Si_2O_5(OH)_4$ (Mg^{2+}:Ni^{2+} = 1.0:1.0) NTs containing multitudes of dislocations, defects, and terraces, and also the synergistic effect of Ni−Mg should contribute to the $(Ni,Mg)_3Si_2O_5(OH)_4$ (Mg^{2+}:Ni^{2+} = 1.0:1.0) NTs supported by 0.045 wt % Pd as a robust reusable high-efficiency catalyst for the selected SM coupling reactions but with extremely low Pd release. The present $(Ni,Mg)_3Si_2O_5(OH)_4$ (Mg^{2+}:Ni^{2+} = 1.0:1.0) solid-solution NTs provided an ideal hydrothermally stable tubular-structured support for Pd and other noble- or transition-metal catalysts with low loading, good recycling, and extremely low ppb level release, which could also be extended as robust reusable high-efficiency catalysts for some other SM coupling reactions.

ASSOCIATED CONTENT

Supporting Information

GC, MS, and XPS spectra and tables of ICP-MS and GC yield results and TON and TOF values. This material is available free of charge via the Internet at http://pubs.acs.org.

AUTHOR INFORMATION

Corresponding Author

*E-mail: wangxun@mail.tsinghua.edu.cn. Tel: 86-10-62792791.

Notes

The authors declare no competing financial interest.

ACKNOWLEDGMENTS

This work was supported by NSFC (Grants 91127040, 20971078, and 20921001) and the State Key Project of Fundamental Research for Nanoscience and Nanotechnology (Grant 2011CB932402). The authors thank Dr. Yiqing Zhou and Dr. Guirong Zhang at the Department of Chemistry, Tsinghua University, for helpful discussion and also the reviewers for constructive suggestions on the great improvement of this work.

REFERENCES

(1) Heck, R. F. *J. Am. Chem. Soc.* **1968**, *90*, 5518.
(2) Heck, R. F. *Acc. Chem. Res.* **1979**, *12*, 146.
(3) Beletskaya, I. P.; Cheprakov, A. V. *Chem. Rev.* **2000**, *100*, 3009.
(4) Negishi, E.; Hu, Q.; Huang, Z.; Qian, M.; Wang, G. *Aldrichim. Acta* **2005**, *38*, 71.
(5) Negishi, E. *Acc. Chem. Res.* **1982**, *15*, 340.
(6) Rafael, C.; Carmen, N. *Chem. Rev.* **2007**, *107*, 874.
(7) Li, P.; Wang, L.; Li, H. *Tetrahedron* **2005**, *61*, 8633.
(8) Yin, L.; Liebscher, J. *Chem. Rev.* **2007**, *107*, 133.
(9) Fihri, A.; Bouhrara, M.; Nekoueishahraki, B.; Basset, J.-M.; Polshettiwar, V. *Chem. Soc. Rev.* **2011**, DOI: 10.1039/c1cs15079k.
(10) Lamblin, M.; Nassar-Hardy, L.; Hierso, J.-C.; Fouquet, E.; Felpin, F.-X. *Adv. Synth. Catal.* **2010**, *352*, 33.
(11) Bellina, F.; Carpita, A.; Rossi, R. *Synthesis* **2004**, *15*, 2419.
(12) Kotha, S.; Lahiri, K.; Kashinath, D. *Tetrahedron* **2002**, *58*, 9633.
(13) Alonso, F.; Beletskaya, I. P.; Yus, M. *Tetrahedron* **2008**, *64*, 3047.
(14) Franzén, R.; Xu, Y. *Can. J. Chem.* **2005**, *83*, 266.
(15) Molnar, A. *Chem. Rev.* **2011**, *111*, 2251.
(16) Seki, M. *Synthesis* **2006**, *18*, 2975.
(17) Alonso, F.; Beletskaya, I. P.; Yus, M. *Tetrahedron* **2005**, *61*, 11771.
(18) Biffis, A.; Zecca, M.; Basato, M. *J. Mol. Catal. A: Chem.* **2001**, *173*, 249.
(19) Cheong, S.; Watt, J. D.; Tilley, R. D. *Nanoscale* **2010**, *2*, 2045.
(20) Beller, M.; Fischer, H.; Kühlein, K.; Reisinger, C.-P.; Herrmann, W. A. *J. Organomet. Chem.* **1996**, *520*, 257.
(21) Zhao, F.; Murakami, K.; Shirai, M.; Arai, M. *J. Catal.* **2000**, *194*, 479.
(22) Reetz, M. T.; Breinbauer, R.; Wannlnge, K. *Tetrahedron Lett.* **1996**, *37*, 4499.
(23) Okumura, K.; Matsui, H.; Sanada, T.; Arao, M.; Honma, T.; Hirayama, S.; Niwa, M. *J. Catal.* **2009**, *265*, 89.
(24) Yang, Y.; Liang, Q.; Li, J.; Zhuang, Y.; He, Y.; Bai, B.; Wang, X. *Nano Res.* **2011**, *4*, 882.
(25) Wang, X.; Zhuang, J.; Chen, J.; Zhou, K.; Li, Y. *Angew. Chem., Int. Ed.* **2004**, *43*, 2017.
(26) Li, R.; Tao, X.; Li, X. *J. Mater. Chem.* **2009**, *19*, 983.

(27) Zhang, L.; Wang, L.; Li, H.; Li, P. *Synth. Commun.* **2008**, *38*, 1498.
(28) Pan, H.-B.; Yen, C. H.; Yoon, B.; Sato, M.; Wai, C. M. *Synth. Commun.* **2006**, *36*, 3473.
(29) Cui, Y.-C.; Zhao, X.-W.; Zhang, J.-W.; Zhang, L.; Liu, X.-M. *Acta Chim. Sin.* **2006**, *64*, 42.
(30) Chandrasekhar, V.; Suriya Narayanan, R.; Thilagar, P. *Organometallics* **2009**, *28*, 5883.
(31) Cai, M.; Sha, J.; Xu, Q. *J. Mol. Catal A: Chem.* **2007**, *268*, 82.
(32) Artner, J.; Bautz, H.; Fan, F.; Habicht, W.; Walter, O.; Döring, M.; Arnold, U. *J. Catal.* **2008**, *255*, 180.
(33) Bergbreiter, D. E.; Osburn, P. L.; Wilson, A.; Sink, E. M. *J. Am. Chem. Soc.* **2000**, *122*, 9058.
(34) Chen, X.; Hou, Y.; Wang, H.; Cao, Y.; He, J. *J. Phys. Chem. C* **2008**, *112*, 8172.
(35) Baldan, A. *J. Mater. Sci.* **2002**, *37*, 2171.
(36) *Handbook of X-ray Photoelectron Spectroscopy*; JF, M., WF, S., PE, S., KD, B., Eds.; Perkin-Elmer Corp.: Eden Prairie, MN, 1992; Vol. 3.
(37) Semagina, N.; Renken, A.; Laub, D.; Kiwi-Minsker, L. *J. Catal.* **2007**, *246*, 308.
(38) Takasu, Y.; Unwin, R.; Tesche, B.; Bradshaw, A. M.; Grunze, M. *Surf. Sci.* **1978**, *77*, 219.
(39) Bulut, H.; Artoka, L.; Yilmaz, S. *Tetrahedron Lett.* **2003**, *44*, 289.
(40) Webb, J. D.; MacQuarrie, S.; McEleney, K.; Crudden, C. M. *J. Catal.* **2007**, *252*, 97.
(41) Gulay, D.; Ozge, A.; Levent, A. *J. Mol. Catal. A: Chem.* **2007**, *278*, 189.
(42) Zhang, X.; Shi, H.; Xu, B.-Q. *Catal. Today* **2007**, *122*, 330.
(43) Zhang, X.; Shi, H.; Xu, B.-Q. *Angew. Chem., Int. Ed.* **2005**, *44*, 7132.
(44) Umpierre, A. P.; Jesus, E. d.; Dupont, J. *ChemCatChem* **2011**, *3*, 1413.
(45) Chen, J.-S.; Vasiliev, A. N.; Panarello, A. P.; Khinast, J. G. *Appl. Catal., A* **2007**, *325*, 76.
(46) Crudden, C.; Sateesh, M.; Lewis, R. *J. Am. Chem. Soc.* **2005**, *127*, 10045.
(47) Hoshiya, N.; Shimoda, M.; Yoshikawa, H.; Yamashita, Y.; Shuto, S.; Arisawa, M. *J. Am. Chem. Soc.* **2010**, *132*, 7270.
(48) Qin, Y.; Wei, W.; Luo, M. *Synlett* **2007**, *15*, 2410.
(49) Widegren, J. A.; Finke, R. G. *J. Mol. Catal. A: Chem.* **2003**, *198*, 317.
(50) Weddle, K. S.; Aiken, J. D., III; Finke, R. G. *J. Am. Chem. Soc.* **1998**, *120*, 5653.
(51) Wolfe, J. P.; Singer, R. A.; Yang, B. H.; Buchwald, S. L. *J. Am. Chem. Soc.* **1999**, *121*, 9550.
(52) Dupont, J.; Consorti, C. S.; Spencer, J. *Chem. Rev.* **2005**, *105*, 2527.
(53) Phan, N. T. S.; Sluys, M. V. D.; Jones, C. W. *Adv. Synth. Catal.* **2006**, *348*, 609.
(54) Conlon, D. A.; Pipik, B.; Ferdinand, S.; LeBlond, C. R.; Sowa, J. R.; Izzo, J. B.; Collins, P.; Ho, G.-J.; Williams, J. M.; Shi, Y.-J.; Sun, Y. *Adv. Synth. Catal.* **2003**, *345*, 931.
(55) Kantam, M. L.; Roy, S.; Roy, M.; Sreedhar, B.; Choudary, B. M. *Adv. Synth. Catal.* **2005**, *347*, 2002.
(56) Polshettiwar, V.; Nadagouda, M. N.; Varma, R. S. *Chem. Commun.* **2008**, 6318.
(57) Kim, J.-H.; Kim, J.-W.; Shokouhimehr, M.; Lee, Y.-S. *J. Org. Chem.* **2005**, *70*, 6714.

dx.doi.org/10.1021/ic2024378 | *Inorg. Chem.* 2012, 51, 6020−6031